

Hierarchical Residual Attention Network for Single Image Super-Resolution

Parichehr Behjati
Computer vision center
Barcelona, Catalonia Spain
pbehjati@cvc.uab.es

Pau Rodríguez
Element AI
Montreal, Canada

Armin Mehri
Computer Vision Center
Barcelona, Catalonia Spain

Isabelle Hupont
Herta Security
Barcelona, Catalonia Spain

Carles Fernández Tena
Herta Security
Barcelona, Catalonia Spain

Jordi González
Computer Vision Center
Barcelona, Catalonia Spain

Convolutional neural networks are the most successful models in single image super-resolution. Deeper networks, residual connections, and attention mechanisms have further improved their performance. However, these strategies often improve the reconstruction performance at the expense of considerably increasing the computational cost. This paper introduces a new lightweight super-resolution model based on an efficient method for residual feature and attention aggregation. In order to make an efficient use of the residual features, these are hierarchically aggregated into feature banks for posterior usage at the network output. In parallel, a lightweight hierarchical attention mechanism extracts the most relevant features from the network into attention banks for improving the final output and preventing the information loss through the successive operations inside the network. Therefore, the processing is split into two independent paths of computation that can be simultaneously carried out, resulting in a highly efficient and effective model for reconstructing fine details on high-resolution images from their low-resolution counterparts. Our proposed architecture surpasses state-of-the-art performance in several datasets, while maintaining relatively low computation and memory footprint.

1. Introduction

Single image super-resolution (SISR) is the task of reconstructing a high-resolution image (HR) from its low-resolution version (LR). This task is ill-posed, as multiple HR images can map to the same LR input. To tackle this inverse problem, numerous techniques have been proposed, including early interpolation [41], reconstruction-based methods [39] or, more recently, learning-based methods [1, 7, 26]. The development of convolutional neural networks (CNNs) followed by residual learning have paved the way for numerous advances in SISR. Most CNN-based

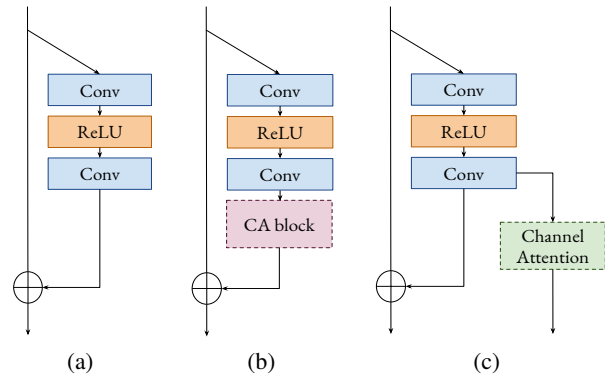


Figure 1: (a) Basic residual block without attention mechanisms. (b) Channel-wise attention (CA) residual block proposed in previous works. (c) Our proposed channel attention mechanism with its own dedicated computational path.

SR methods employ a massive number of stacked residual blocks, as shown in Figure 1 (a), which allows deeper networks and a great increase in performance.

In spite of their outstanding performance, most SR deep networks still face some limitations. Usually, SR models are built by successively stacking residual blocks. Under this design, the residual features from preceding blocks must go through a long path to propagate until the final blocks, as these features are repeatedly merged with identity features to form more complex ones during transmission. Therefore, highly representative residual features are mostly computed locally, and lost in the residual addition during the learning process of the entire network. Moreover, very deep networks dramatically increase computational demands and memory consumption, which limits the use of modern architectures in real-world scenarios, such as mobile devices. To tackle these problems, some SR methods focus on lightweight architecture designs such as pyra-

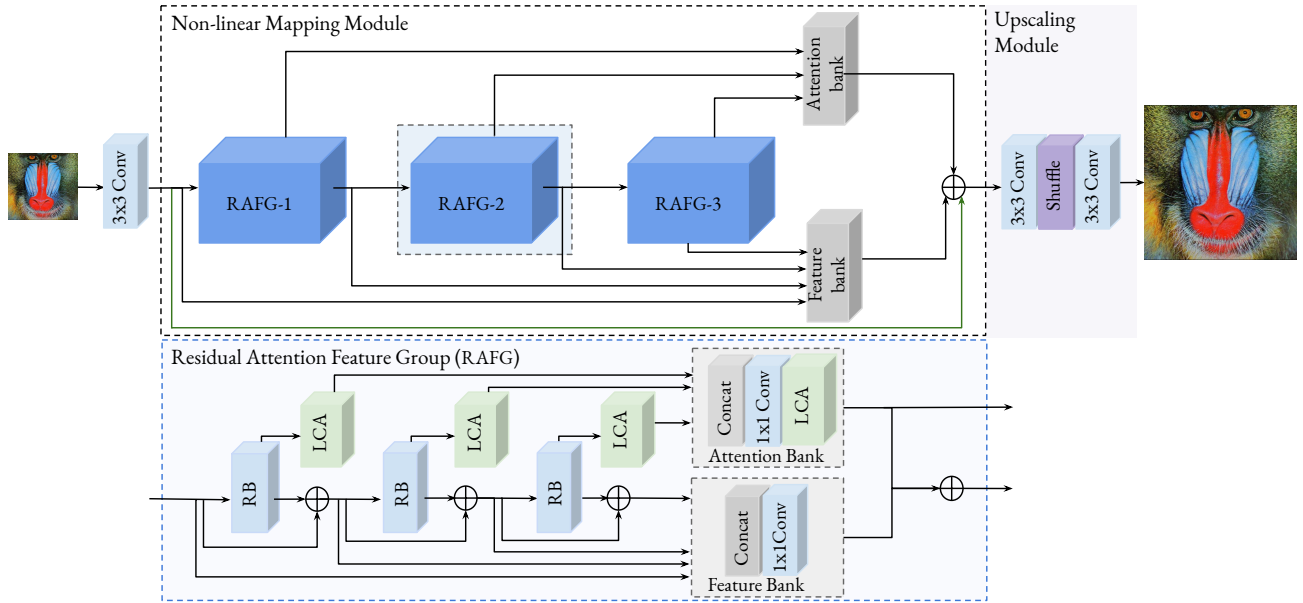


Figure 2: **Top:** Proposed Hierarchical Residual Attention Network (HRAN) architecture for SISR. **Bottom:** Residual Attention Feature Group (RAFG), containing residual blocks (RB) and lightweight channel attention (LCA) blocks

mid networks [18], recursive operations with weight sharing [1, 3, 5], neural architecture search [14, 15] and channel grouping [6] to reduce the number of network parameters. Another problem of CNN-based SR methods as [21, 41] is that they are not explicitly designed to pay attention to the precious high-frequency information that must be reconstructed from the LR inputs. Previous works address this problem by re-weighting feature channels with channel attention [25, 26, 42]. However, channel attention may discard relevant details that will no longer be available at deeper levels of the neural architecture. Although attention-based approaches usually achieve better performance, they often increase model complexity and computational cost. Moreover, these methods were originally crafted for high-level vision problems such as image classification, so they do not take into account the particularities of SISR, like the need of preserving high-frequency components from LR inputs. In addition to this, how to effectively compute a multi-level feature representations for restoring high quality HR images within the network is of also crucial importance, yet it remains to be explored.

To confront these issues and address the problem of feature degradation, we introduce Residual Attention Feature Groups (RAFGs). The proposed RAFG is composed of a collection of stacked residual blocks. The output of each residual block is linearly fused at the RAFG output in order to take into account the whole feature hierarchy, to minimize the information loss during processing through the network, and to ease the gradient flow for optimization [13]. This way, each residual block can focus on different aspects

of the original LR input.

However, using these stacked residual blocks solely is not sufficient to increase network’s sensitivity towards information-rich channels. A number of previous approaches have tackled this challenge by performing in-place channel attention within the residual blocks, as in Figure 1 (b), to further boost the representational ability of the network. Nevertheless, such *in-place* attention mechanisms may discard relevant details that will no longer be available at deeper levels of the architecture. To solve this problem, and in contrast to previous approaches, the proposed RAFG is designed to combine lightweight channel attention blocks with residual blocks by keeping a dedicated computational path for attention modules. Figure 1 (c) shows that using RAFG, attention modules are independent from the purely residual path, and parallel to it. As a result, they are able to attend to relevant features while preserving higher frequency details across the whole network.

To verify the effectiveness of the proposed RAFG, we build upon them a deep architecture for SISR named Hierarchical Residual Attention Network (HRAN), illustrated in Figure 2. Our experiments show that our network outperforms previous state-of-the-art approaches in standard benchmarks, while maintaining low computation and memory requirements. In summary, the main contributions of this paper are as follows:

1. We introduce a novel procedure for using channel attention mechanisms together with residual blocks, following two independent but parallel computational

paths. The idea is to hierarchically aggregate their respective contributions across the network, using Residual Attention Feature Groups to facilitate the preservation of finer details.

2. To demonstrate the potential of the proposed attention mechanism, we present the Hierarchical Residual Attention Network (HRAN), a deep architecture for SISR grounded on the use of RAFGs. Extensive experiments on a variety of public datasets demonstrate the superiority of the proposed architecture over state-of-the-art models.
3. As a consequence of the previous, we obtain a lightweight and efficient SISR model, in which features and attention are processed simultaneously, thus improving the performance while reducing memory and processing costs.

2. Related Work

2.1. Evolution of Architectures for SISR

Dong et al. [8] first proposed SRCNN, a shallow neural network to predict the non-linear relationship between bicubic upsamplings and HR images. SRCNN has a large number of operations compared to its depth, as it extracts features from upsampled LR images. In contrast, FSCRNN [9] and ESPCN [21] started to directly adopt the LR image as input by adding a single transposed convolution layer to produce the final HR output, which lead to a reduction in the number of operations when compared to SRCNN. These early methods are considered shallow models.

Subsequent approaches have shown better performances than shallow models by using deep neural networks [34]. VDSR [16] and IRCNN [40] improved the performance by increasing the network depth, using stacked convolutions with residual connections. Lim et al. [21] further expanded the network size and improved residual blocks by removing batch normalization layers. Furthermore, to effectively send information across layers, dense blocks [13] were employed in several SR deep networks [33, 36, 43]. In MemNet, Tai et al. [32] designed memory blocks also based on dense connections. Meanwhile, to simplify the challenge of directly super-resolving the details, He et al. [11] adopted a progressive structure to reconstruct HR images in a stage-by-stage upscaling manner. Li et al. [20] and Haris et al. [10] incorporated the feedback mechanism into network designs for exploiting both LR and HR signals jointly. Recently, Luo et al. [23] proposed butterfly structures in LatticeNet, combining residual blocks to further improve results. Nevertheless, despite their remarkable performance, such methods demand very high computational cost and memory requirements.

Numerous lightweight models have been proposed to alleviate the computational burden. For example, DRCN [17] was the first to apply recursive algorithms to SISR to reduce the number of parameters. Kim et al. [17] revisited DRCN by combining recursive structures and residual blocks so as to improve performance with even fewer parameters. Likewise, Ahn et al. [1], Behjati et al. [3] also joined residual connections and recursive layers to reduce the computational cost. Chu et al. [6] introduced Neural Architecture Search (NAS) strategies to automatically build an SR model given certain constraints. Zhu and Zhao [45] proposed CBPN, an efficient version of the DBPN network [10], which emphasizes high-resolution features present in LR images. Very recently, Muqet et al. [25] proposed an architecture based on sequentially stacked residual blocks. All the aforementioned works demonstrate that lightweight SR networks are capable of providing good trade-offs between performance and number of parameters.

2.2. Attention Mechanisms in SISR

The aim of introducing attention mechanisms to neural networks is to re-calibrate the feature responses towards the most informative and important components of the inputs. In short, they help the network ignore irrelevant information and focus on the important one [12, 29]. For example, Woo et al. [37] stacked spatial and channel-wise attention modules at multiple layers for image classification. Attention mechanisms have also been successfully applied to deep CNN-based image enhancement methods and, more particularly, to SISR. Zhang et al. [42] first proposed a very deep residual channel attention network (RCAN), which integrated channel-wise attention into residual blocks and pushed the state-of-the-art performance of SISR.

Only very recently, SISR works have started to investigate more sophisticated attention mechanisms, leaving room for further research in field. Liu et al. [22] proposed enhanced spatial attention (ESA), a combined solution for channel and spatial attention, which reduces the number of channels using 1×1 convolutions and shrinks spatial dimensions via strided convolutions. Inspired by ESA, Muqet et al. [25] presented a cost-efficient attention mechanism (CEA) introducing dilated convolutions with different filter sizes. Niu et al. [26] proposed a layer and channel-wise attention mechanism to selectively capture more informative features. Meanwhile, Mehri et al. [24] proposed to combine both channel-wise and spatial attentions to learn more expressive context information. Another example is the work by Zhao et al. [44], which introduces a pixel-wise channel attention to produce 3D attention maps.

3. Hierarchical Residual Attention Network

In this section, we first provide an overview of the proposed Hierarchical Residual Attention Network (HRAN)

for SISR. Then, we detail the components of a residual attention feature group (RAFG).

3.1. HRAN Overview

As shown in Figure 2, HRAN consists of a non-linear mapping module and a final upscaling and image reconstruction module. Let’s denote I_{LR} and I_{SR} the input and output of HRAN, respectively. As recommended in [19, 21], we apply only one 3×3 convolutional layer to extract the initial features F_0 from the LR input image:

$$F_0 = \text{Conv}_{3 \times 3}(I_{LR}) \quad (1)$$

Next, the extracted features F_0 are sent to the non-linear mapping module, which computes useful representations of the LR patch in order to infer its HR version. Note that we also introduce a long-range skip connection to grant access to the original information and facilitate the back-propagation of the gradients (green connection in Figure 2).

Let F be the output of the non-linear mapping module, further detailed in Section 3.2, which contains high resolution features. Then, an upscaling process grounded on a sub-pixel shuffle convolutional layer [30] is applied:

$$F^\uparrow = \text{sub-pixelshuffle}(F). \quad (2)$$

The upscaled features F^\uparrow are finally mapped into the SR image I_{SR} via one convolutional layer:

$$I_{SR} = \text{Conv}_{3 \times 3}(F^\uparrow). \quad (3)$$

To optimize HRAN and following previous works, we adopt the L_1 loss as a cost function for training. Given a training set with N pairs of LR images and HR counterparts, denoted by $\{I_{LR}^i, I_{HR}^i\}_{i=1}^N$, HRAN is optimized to minimize the L_1 loss function:

$$L(\theta) = \frac{1}{N} \sum_{i=1}^N \|I_{LR}^i - I_{HR}^i\|_1, \quad (4)$$

where θ denotes the parameter set of HRAN.

3.2. Residual Attention Feature Group

The residual attention feature group (RAFG) is the core of the non-linear mapping module. It is designed to attend and preserve higher frequency details across the whole network. As shown in Figure 2 (bottom), it is composed of two dedicated computational paths: (i) feature banks and (ii) attention banks. We detail each of these below.

Feature banks. In essence, residual features are linearly combined at banks which are built by aggregating all the features from previous residual blocks. As a result, these banks capture detailed information from features across the whole architecture, thus reducing feature degradation

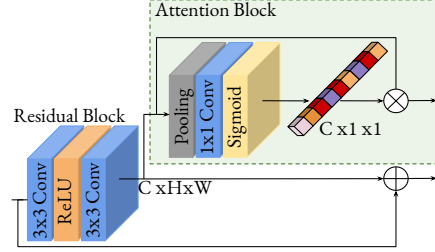


Figure 3: Proposed mechanism for extracting channel-wise attention from residual blocks.

and boosting the network’s overall representational ability. Given that the systematic concatenation of features results in redundant information, we also incorporate 1×1 bottleneck convolutions after feature aggregation.

Compared to a simple stacking of multiple residual blocks, the use of hierarchical banks enables a non-local exploitation of residual features. Although stacked residual blocks facilitate the task of training deeper SISR networks, residual feature information gradually disappears during the transmission and residual blocks play a very local role in the learning process of the whole network. This is because residual features from preceding blocks must go through a long path to propagate to subsequent ones.

In contrast, with feature banks, information from preceding residual blocks can be hierarchically propagated bottom-up without any loss or interference, thus leading to a more discriminative feature representation.

Lightweight Channel Attention (LCA) blocks. To further improve the performance of HRAN, we also propose the use of LCA blocks. Their structure is illustrated in Figure 3. The attention recalibrates feature responses by implicitly modeling interdependencies between channels. In order to make it efficient, we propose to use a single 1×1 convolutional layer instead of the two 1×1 bottleneck convolutions commonly used in the literature [42]. Formally, we denote $u = [u_1, \dots, u_C]$ the input of the LCA block, which consists of C feature maps u_i of spatial size $H \times W$. These feature maps are first reduced in the spatial dimension by an average pooling operation:

$$z_c = \frac{1}{H \times W} \sum_{i=1}^H \sum_{j=1}^W u_c(i, j), \quad (5)$$

where $u_c(i, j)$ is the value at position (i, j) of the c -th channel, and z_c is the value obtained for channel c after average pooling. To attend to the most relevant feature maps, we employ a gating mechanism with sigmoid activation:

$$\alpha_c = \sigma(W_{LCA} * z_c), \quad (6)$$

where σ represents the sigmoid function, $z = [z_1, \dots, z_C]$, and $*$ denotes a linear transformation with $C \times C$ weights

W_{LCA} . The final channel importance weights $\alpha = [\alpha_1, \dots, \alpha_C]$ are used to re-scale the input u :

$$\tilde{u}_c = \alpha_c \cdot u_c \quad (7)$$

Integrating LCA in HRAN. The features extracted by a deep network contain different types of information in each channel. If we are able to increase the network’s sensitivity to information-rich channels and make it focus on them, the efficiency of the network will be enhanced and its performance improved. In the literature, channel attention mechanisms have been one of the most successful strategies for this purpose. Previous approaches performed channel attention *in-place* inside the residual blocks to further boost the representational ability of the network [12]. This usually implied an element-wise product between the attention output and the residual block output. However, this in-place channel attention may discard relevant details which will no longer be available in deeper levels of the architecture.

In our approach, we propose to keep a dedicated computational path for attention modules, independent from the aggregation of residual features, and parallel to it. Figure 2 (bottom) shows that a RAFG contains three residual blocks, the output of which are respectively sent to an LCA block before element-wise addition. Attention outputs are then globally aggregated as a bank of attentions, and the same happens with the residual features, which are globally combined as a bank of features. The attention bank additionally incorporates an extra LCA block, which helps to efficiently extract the most important components of the feature hierarchy. Finally, the outputs of both banks are combined together and sent to the subsequent RAFG. Likewise, the outputs of all the feature banks and attention banks are combined by a final, higher-level feature bank and attention bank at the output of the network.

4. Experimental Results

In this section, we first compare our HRAN with state-of-the-art algorithms on five benchmark datasets. We then analyze the contributions of the proposed channel attention mechanism and residual attention feature group.

4.1. Settings

Datasets. Following [22, 25, 26], we use 800 high-quality training images from DIV2K dataset as our training set. Several benchmark datasets are used for testing, namely Set5 [4], Set14 [38], B100 [2], and Urban100 [2], each with diverse characteristics. We perform our experiments with bicubic (BI) and blur-downscale (BD) degradation models. All the results are evaluated with two commonly used metrics: PSNR (peak-to-noise-ratio) and SSIM (structural similarity index), on the Y channel of the YCbCr space.

Implementation details. During training, data augmentation is carried out by means of random horizontal flips and 90° rotation. At each training mini-batch, 64 LR RGB patches with size 64×64 are provided as inputs. We train an HRAN consisting of 3 RAFGs, each with 3 residual blocks (RBs) and 3 attention modules (LCAs). We train our models using the ADAM optimizer with learning rate set to the maximum convergent value (10^{-3}), applying weight normalization in all convolutional layers. The learning rate is decreased by half every 2×10^5 back-propagation iterations. The proposed architecture has been implemented using PyTorch [27], and trained on NVIDIA 1080 Ti GPUs¹.

4.2. Comparison with State-of-the-art Methods

Simulating LR image with bicubic (BI) and blur-downscale (BD) degradation models is a common practice in SISR. In this section we report results using both strategies. We also present a comparative visual analysis of our proposed attention mechanism, and study HRAN’s computational performance with regard to state-of-the-art SISR models.

4.2.1 Results with BI Degradation Models

We compare HRAN with 11 lightweight state-of-the-art methods [1, 3, 15, 16, 20, 23, 24, 25, 31, 32, 44]. For fair comparison, we train models individually for each scale factor, including $\times 2$, $\times 3$ and $\times 4$. We evaluate our model on different benchmarks using PSNR and SSIM as metrics.

Table 1 shows quantitative evaluation results, including the number of parameters for a more informative comparison. Note that in this table we only compare models that have a roughly similar number of parameters as ours. Compared to existing methods, and without using self-ensemble, our network is the best performing one at all scales. HRAN attains remarkable performance in all datasets including Urban100, which contains rich structure contents. This confirms that HRAN is able to gradually aggregate, select and preserve relevant details across the whole network. These quantitative results also translate into more accurate reconstructions in Figure 4, demonstrating that our method is able to generate clearer structures and details.

4.2.2 Results with BD Degradation Model

Following [3, 7, 24, 43], we also provide the results after applying a BD degradation model. We compare our proposed method with 8 state-of-the-art-methods [3, 8, 9, 16, 24, 28, 33, 40]. Because of the mismatch of the degradation setups, SRCNN, FSRCNN and VDSR have been re-trained. As shown in Table 2, HRAN achieves the best PSNR and SSIM scores compared to other SR methods on all the datasets.

¹The code is publicly available at: (blind for review process)

Table 1: Average PSNR/SSIM values for models with the same order of magnitude of parameters. Performance is shown for scale factors $\times 2$, $\times 3$ and $\times 4$ with **BI** degradation. The number of parameters and of each method are indicated under their name. The best performance is shown **highlighted** and the second best underlined.

Dataset	Scale	VDSR 0.7M	DRNN 0.3M	MemNet 0.7M	CARN 1.6M	SRFBN_s 0.5M	IMDN 0.7	PAN 0.3M	MAFFSRN_L 0.8M	LatticeNet 0.8M	MPRNet 0.5M	OverNet 0.9M	Ours 0.9M
Set5	$\times 2$	37.53/0.9587	37.74/0.9591	37.78/0.9597	37.76/0.9590	38.02/0.9605	38.00/0.9605	38.00/0.9605	38.07/0.9607	<u>38.15/0.9610</u>	38.08/0.9608	38.11/0.9610	38.23/0.9616
	$\times 3$	33.66/0.9213	34.03/0.9244	34.09/0.9248	34.29/0.9255	34.20/0.9255	34.36/0.9270	34.40/0.9271	34.45/0.9277	34.53/0.9281	<u>34.57/0.9285</u>	34.49/0.9267	34.62/0.9288
	$\times 4$	31.35/0.8838	31.68/0.8888	31.74/0.8893	32.13/0.8937	31.98/0.8923	32.21/0.8948	32.13/0.8948	32.20/0.8953	32.30/0.8962	<u>32.38/0.8969</u>	32.32/0.8956	32.50/0.8976
Set14	$\times 2$	33.03/0.9124	33.23/0.9136	33.28/0.9142	33.52/0.9166	33.35/0.9156	33.63/0.9177	33.59/0.9181	33.59/0.9177	33.78/0.9193	<u>33.79/0.9196</u>	33.71/0.9179	33.81/0.9198
	$\times 3$	29.77/0.8314	29.96/0.8349	30.00/0.8350	30.29/0.8407	30.10/0.8372	30.32/0.8417	30.36/0.8423	30.40/0.8432	30.39/0.8424	<u>30.42/0.8441</u>	<u>30.47/0.8436</u>	30.55/0.8449
	$\times 4$	28.01/0.7674	28.21/0.7720	28.26/0.7723	28.60/0.7806	28.45/0.7779	28.58/0.7811	28.61/0.7822	28.62/0.7822	28.68/0.7830	<u>28.69/0.7841</u>	<u>28.71/0.7826</u>	28.76/0.7848
B100	$\times 2$	31.90/0.8960	32.05/0.8973	32.08/0.8978	32.09/0.8978	32.20/0.9000	32.19/0.8996	32.18/0.8997	32.23/0.9005	<u>32.25/0.9005</u>	<u>32.25/0.9004</u>	32.24/0.9007	32.31/0.9011
	$\times 3$	28.82/0.7976	28.95/0.8004	28.96/0.8001	29.06/0.8034	29.11/0.8085	29.09/0.8046	29.11/0.8050	29.13/0.8061	29.15/0.8059	<u>29.17/0.8037</u>	<u>29.17/0.8036</u>	29.26/0.8043
	$\times 4$	27.29/0.7251	27.38/0.7284	27.40/0.7281	27.58/0.7349	27.60/0.7369	27.56/0.7353	27.59/0.7363	27.59/0.7370	27.62/0.7367	<u>27.63/0.7385</u>	<u>27.67/0.7383</u>	27.70/0.7399
Urban100	$\times 2$	30.76/0.9140	31.23/0.9188	31.31/0.9195	31.92/0.9256	31.41/0.9207	32.17/0.9283	32.01/0.9273	32.38/0.9308	32.43/0.9302	<u>32.52/0.9317</u>	32.44/0.9311	32.60/0.9322
	$\times 3$	27.14/0.8279	27.53/0.8378	27.56/0.8376	28.06/0.8493	26.41/0.8064	28.17/0.8519	28.11/0.8511	28.26/0.8552	28.33/0.8538	<u>28.42/0.8578</u>	28.37/0.8572	28.57/0.8581
	$\times 4$	25.18/0.7524	25.44/0.7638	25.50/0.7630	26.07/0.7837	24.60/0.7258	26.04/0.7838	26.11/0.7854	26.16/0.7887	26.25/0.7873	<u>26.31/0.7921</u>	<u>26.31/0.7923</u>	26.39/0.7926

Table 2: Average PSNR/SSIM for models with the same order of magnitude of parameters. Scores shown for scale factor $\times 3$ using **BD** degradation model. Best performance is **highlighted**, second best underlined.

DB	Bicubic	SPMSR	SRCNN	FSRCNN	VDSR	IRCNN_G	IRCNN_C	SRMD(NF)	MPRNet	OverNet	Ours
Set5	28.34/0.8161	32.21/0.9001	31.75/0.8988	26.25/0.8130	33.78/0.9198	33.38/0.9182	29.55/0.8246	34.09/0.9242	34.57/0.9278	<u>34.59/0.9279</u>	34.66/0.9281
Set14	26.12/0.7106	28.97/0.8205	28.72/0.8024	25.63/0.7312	29.90/0.8369	29.73/0.8292	27.33/0.7135	30.11/0.8304	<u>30.47/0.8427</u>	30.46/0.8310	30.52/0.8429
B100	26.02/0.6733	28.13/0.7740	27.97/0.7921	24.88/0.6850	28.70/0.80035	28.65/0.7922	26.46/0.6572	28.98/0.8009	<u>29.19/0.8062</u>	29.13/0.8060	29.25/0.8065
Urban100	23.20/0.6661	25.84/0.7856	25.50/0.7812	22.14/0.6815	26.80/0.8191	26.81/0.8189	24.89/0.7172	27.50/0.8370	<u>28.31/0.8538</u>	28.24/0.8485	28.39/0.8541

The consistently better results of HRAN indicate that our method can adapt well to scenarios with multiple degradation models. Figure 5 provides some visual results, where it becomes apparent that the quality of the reconstructions is superior for the proposed method. We found that HRAN is able to recover structured details that were missing the LR image by efficiently exploiting the feature hierarchy.

4.2.3 Visualization of Attention Mechanisms

Figure 6 shows average feature maps of residual blocks, when attention mechanisms are applied within (in-place, top row) or outside (as in our RAFG, bottom row). This visualization shows how RAFGs are able to learn different representations, in contrast to in-place attention. In essence, each RAFG directs computations towards edges and details, thus obtaining a sharper representation at the output. In contrast, when using in-place attention, feature maps vary significantly from the first residual block to the last. As a result, edges and contours are outlined at the first layer, and smooth areas within the original image become suppressed at subsequent blocks.

4.2.4 Model Complexity and Running Time Analysis

In Figure 7 and Figure 8, we compare HRAN against various lightweight and heavy benchmark algorithms respectively, in terms of network parameters and reconstruction PSNR, using the B100 dataset with a scale of $\times 4$. It can be observed that HRAN achieves the best SR results among all lightweight networks. This demonstrates that our method achieves a good trade-off between number of parameters

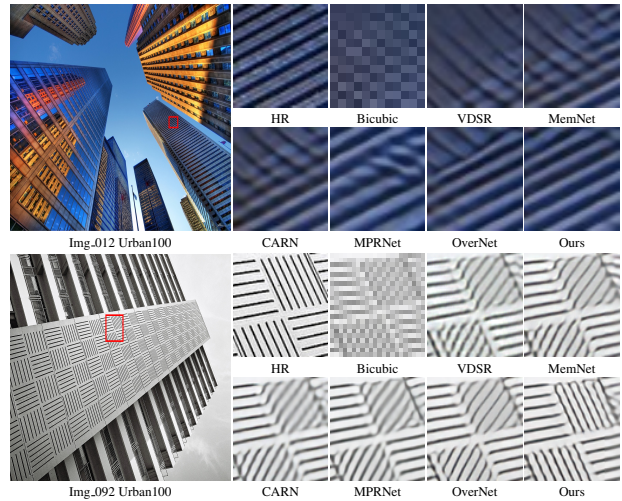


Figure 4: Visual results of **BI** degradation model for $\times 4$ scale factor.

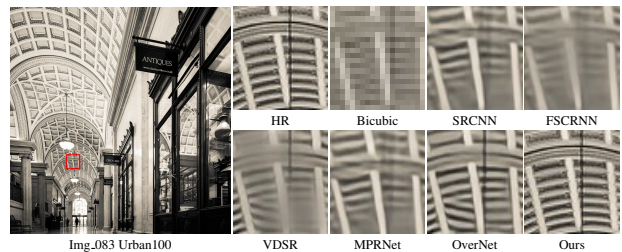


Figure 5: Visual results of **BD** degradation model for $\times 3$ scale factor.

and reconstruction performance. Meanwhile, compared to the networks with larger number of parameters than HRAN, such as EDSR [21] and RDN [43], our proposed method

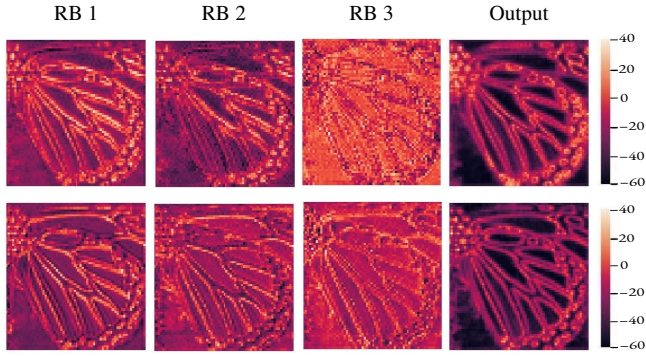


Figure 6: Average feature maps of residual blocks (RBs). **Top**: Attention is applied within the residual (classic approach). **Bottom**: Attention is applied outside the residual (our approach).

achieves competitive or better results with only 2% and 4% the number of parameters of EDSR and RDN, respectively.

Moreover, in Table 3 we compare the running time of HRAN on Urban100 with five other lightweight state-of-the-art networks [3, 15, 20, 24, 32] using a scale factor of $\times 4$. The running time of each network is evaluated on the same machine with a NVIDIA 1080 Ti GPU. We observe that HRAN is the fastest, thus proving its efficiency.

Table 3: Average running time comparison on Urban100 for $\times 4$.

Model	Parameters	Running Time (s)	PSNR
MemNet	0.6M	0.481	25.54
SRFBN_S	0.4M	0.006	25.71
IMDN	0.7M	0.006	26.04
MPRNet	0.5M	0.009	26.31
OverNet	0.9M	0.004	26.31
Ours	0.9M	0.003	26.39

4.3. Ablation Study

4.3.1 Comparing Attention Schemes

To demonstrate the effectiveness of our channel attention, we use HRAN as the basic network, and then replace our attention scheme with channel attention (CA) [35], efficient channel attention (ECA) [42] and pixel-wise channel attention (PA) [44], respectively. Note that we only compare LCA with attention mechanisms that have a similar model complexity. As shown in Figure 1 (c), the channel attention module feeds from the residual block but splits out from it through a dedicated computational path. We train all the aforementioned methods using the same architectural pattern.

Table 4 compares the performance of all methods in terms of PSNR. It can be observed that LCA outperforms the rest of attention methods. Compared with CA, our proposed attention mechanism attains better performance by up to 0.9 dB, arguably because LCA avoids dimensionality reduction, thus preventing information loss [35].

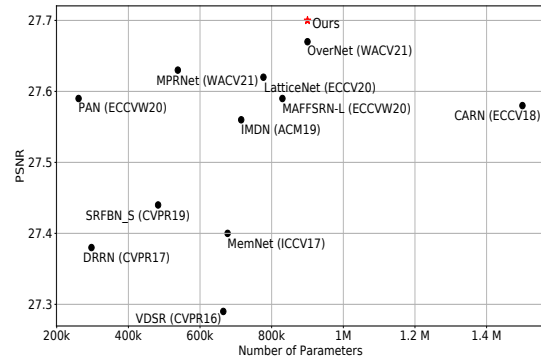


Figure 7: Comparing capacity vs performance for lightweight state-of-the-art SISR models B100 ($\times 4$). The red star represents our method.

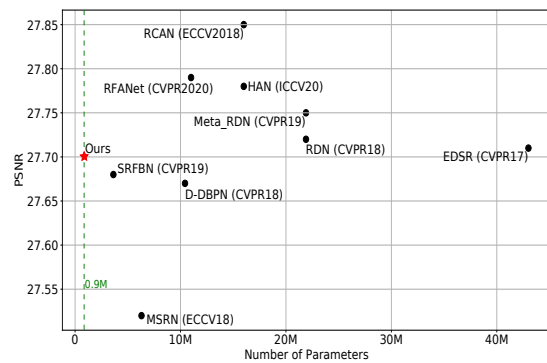


Figure 8: Comparing capacity vs performance for heavy state-of-the-art SISR models on B100 ($\times 4$). The red star represents our method.

4.3.2 Effect of LCA on Existing Models

This section investigates the impact of our proposed channel attention when applied to existing state-of-the-art models. Table 5 shows the performance of applying attention mechanisms including CA [42], ECA [35] and our proposed LCA on EDSR [21] and RCAN [42]. For fair comparison, all the methods are trained on their default settings, and attention mechanisms are performed *in-place*, either at the end of the EDSR blocks or replacing RCAN’s channel attention. We observe that all three attention mechanisms improve the performance of EDSR and RCAN, confirming the importance of attention in SISR tasks.

We also observe that the proposed LCA outperforms CA and ECA on both architectures. We attribute the difference in performance with respect to CA to the fact that CA includes a two 1×1 convolution bottleneck that may lose information during the dimensionality reduction process. ECA follows a similar approach, reducing dimensionality via a 1d convolution on the channel dimension. In contrast, our proposed LCA consists of a single 1×1 convolution that directly maps the input into the attention weights.

4.3.3 Effect of the RAFG

This section discusses the effect of each of the two dedicated computational paths in the proposed RAFG: feature banks and attention banks.

Feature banks. The proposed banks of residuals ensure that informative features from residual blocks can be hierarchically propagated without loss or interference. To verify its performance, we compared the use of hierarchical banks with ResNet, to evaluate the use of a regular architecture composed of several stacked residual blocks. Table 6 shows the results of the experiments, conducted on the Urban100 dataset with scale $\times 4$.

The PSNR of ResNet is 26.03 dB on Urban100, a strong baseline for lightweight SISR methods. When deploying our hierarchical banks of residuals, the PSNR increases to 26.24 dB. Compared to ResNet, the proposed network only incorporates a 1×1 convolution every three residual blocks, yet boosting the PSNR by 0.21 dB. We attribute this considerable improvement to the effectiveness of the proposed connectivity pattern, where the features in each residual block can be better utilized by the network.

Lightweight Channel Attention. Previous SISR approaches perform channel-attention *in-place* within the residual blocks, whereas in this work we take the attention out and compute it in parallel. To verify the effectiveness of this approach, we compare the commonly used in-place attention with our proposed attention mechanism in Table 7. The two models in the table are identical, except that the top row one applies conventional attention within the residual as in Figure 1 (b), and the bottom row one implements our proposal as shown in Figure 1 (c). As it can be observed, our method achieves better results with only a few more parameters, due to the aggregation operation inside the attention feature bank.

4.3.4 Effect of the Feature and Attention Banks

We introduced feature and attention banks at the output of the network in order to grant the reconstruction module access to the full feature hierarchy. In this subsection we study the effectiveness of these banks by directly removing them and only keeping the output of the last RAFG and the long-range skip connection from the input. In Table 8 it can be observed that the proposed banks have a positive impact of almost 0.06 dB on the reconstruction performance of the network. This indicates that the banks successfully discard irrelevant information and distill valuable information from the entire feature hierarchy.

5. Conclusions

We have introduced an efficient architecture (HRAN) for SISR. HRAN is able to extract and preserve fine details from the whole feature hierarchy in order to reduce

Table 4: Average PSNR for attention mechanisms with the same model complexity.

Scale	Attentions	Params	Set14	Urban100
			PSNR/SSIM	PSNR/SSIM
$\times 4$	CA	864K	28.69	26.30
	ECA	871K	28.72	26.34
	PA	918K	28.71	26.32
	LCA	918K	28.76	26.39

Table 5: Effect of attention modules on state-of-the-art methods with scale factor $\times 4$.

Name	EDSR		RCAN	
	Baseline	Attention module	Baseline	Attention module
CA		✓		✓
ECA		✓		✓
LCA		✓		✓
Set5	32.46	32.50 32.52	32.55	32.63 32.67 32.69
Urban100	26.64	26.66 26.69	26.70	26.82 26.86 26.87 26.91

Table 6: Average PSNR for a regular ResNet architecture vs one using the proposed feature banks.

Scale	methods	Params	Set14	Urban100
			PSNR/SSIM	PSNR/SSIM
$\times 4$	ResNet	749K	28.52	26.03
	Ours	814K	28.76	26.24

Table 7: Average PSNR with *in-place* attention and our proposed attention.

Scale	Methods	Params	Set14	Urban100
			PSNR/SSIM	PSNR/SSIM
$\times 4$	in-place	852K	28.69	26.32
	Ours	918K	28.76	26.39

Table 8: Average PSNR obtained with the HRAN model, using or not feature and attention banks at the end of the network.

Scale	Datasets	HRAN w/o banks	HRAN w banks
		Set14	28.71
$\times 4$	B100	27.65	27.70
	Urban100	26.34	26.39

the degradation caused by successive residual aggregations. This is achieved through a novel Residual Attention Feature Group, which combines an efficient dense connectivity pattern with a lightweight channel attention path that is processed in parallel to the main residual computational path. We have empirically shown that the proposed architecture is effective at producing accurate high-resolution reconstructions of the input. As a result, HRAN attains better reconstruction scores on all benchmarks than previous lightweight state-of-the-art models, while having a similar amount of parameters. Through a series of ablation experiments, we have demonstrated the effectiveness of the proposed attention mechanism as well as the RAFGs. We conclude that moving the attention operations outside of the residual blocks is beneficial to prevent the loss of information caused by *in-place* attention.

References

- [1] N. Ahn, B. Kang, and K.-A. Sohn. Fast, accurate, and lightweight super-resolution with cascading residual network. In *Proceedings of the European Conference on Computer Vision (ECCV)*, pages 252–268, 2018.
- [2] P. Arbelaez, M. Maire, C. Fowlkes, and J. Malik. Contour detection and hierarchical image segmentation. *IEEE transactions on pattern analysis and machine intelligence*, 33(5): 898–916, 2010.
- [3] P. Behjati, P. Rodriguez, A. Mehri, I. Hupont, C. F. Tena, and J. Gonzalez. Overnet: Lightweight multi-scale super-resolution with overscaling network. In *Winter Conference on Applications of Computer Vision (WACV2021)*, 2021.
- [4] M. Bevilacqua, A. Roumy, C. Guillemot, and M. L. Alberi-Morel. Low-complexity single-image super-resolution based on nonnegative neighbor embedding. 2012.
- [5] J.-H. Choi, J.-H. Kim, M. Cheon, and J.-S. Lee. Lightweight and efficient image super-resolution with block state-based recursive network. *arXiv preprint arXiv:1811.12546*, 2018.
- [6] X. Chu, B. Zhang, H. Ma, R. Xu, J. Li, and Q. Li. Fast, accurate and lightweight super-resolution with neural architecture search. *arXiv preprint arXiv:1901.07261*, 2019.
- [7] T. Dai, J. Cai, Y. Zhang, S.-T. Xia, and L. Zhang. Second-order attention network for single image super-resolution. In *Proceedings of the IEEE conference on computer vision and pattern recognition*, pages 11065–11074, 2019.
- [8] C. Dong, C. C. Loy, K. He, and X. Tang. Learning a deep convolutional network for image super-resolution. In *European conference on computer vision*, pages 184–199. Springer, 2014.
- [9] C. Dong, C. C. Loy, and X. Tang. Accelerating the super-resolution convolutional neural network. In *European conference on computer vision*, pages 391–407. Springer, 2016.
- [10] M. Haris, G. Shakhnarovich, and N. Ukita. Deep back-projection networks for super-resolution. In *Proceedings of the IEEE conference on computer vision and pattern recognition*, pages 1664–1673, 2018.
- [11] Z. He, S. Tang, J. Yang, Y. Cao, M. Y. Yang, and Y. Cao. Cascaded deep networks with multiple receptive fields for infrared image super-resolution. *IEEE transactions on circuits and systems for video technology*, 29(8):2310–2322, 2018.
- [12] J. Hu, L. Shen, and G. Sun. Squeeze-and-excitation networks. In *Proceedings of the IEEE conference on computer vision and pattern recognition*, pages 7132–7141, 2018.
- [13] G. Huang, Z. Liu, L. Van Der Maaten, and K. Q. Weinberger. Densely connected convolutional networks. In *Proceedings of the IEEE conference on computer vision and pattern recognition*, pages 4700–4708, 2017.
- [14] Z. Hui, X. Wang, and X. Gao. Fast and accurate single image super-resolution via information distillation network. In *Proceedings of the IEEE conference on computer vision and pattern recognition*, pages 723–731, 2018.
- [15] Z. Hui, X. Gao, Y. Yang, and X. Wang. Lightweight image super-resolution with information multi-distillation network. In *Proceedings of the 27th ACM International Conference on Multimedia*, pages 2024–2032, 2019.
- [16] J. Kim, J. Kwon Lee, and K. Mu Lee. Accurate image super-resolution using very deep convolutional networks. In *Proceedings of the IEEE conference on computer vision and pattern recognition*, pages 1646–1654, 2016.
- [17] J. Kim, J. Kwon Lee, and K. Mu Lee. Deeply-recursive convolutional network for image super-resolution. In *Proceedings of the IEEE conference on computer vision and pattern recognition*, pages 1637–1645, 2016.
- [18] W.-S. Lai, J.-B. Huang, N. Ahuja, and M.-H. Yang. Deep laplacian pyramid networks for fast and accurate super-resolution. In *Proceedings of the IEEE conference on computer vision and pattern recognition*, pages 624–632, 2017.
- [19] C. Ledig, L. Theis, F. Huszár, J. Caballero, A. Cunningham, A. Acosta, A. Aitken, A. Tejani, J. Totz, Z. Wang, et al. Photo-realistic single image super-resolution using a generative adversarial network. In *Proceedings of the IEEE conference on computer vision and pattern recognition*, pages 4681–4690, 2017.
- [20] Z. Li, J. Yang, Z. Liu, X. Yang, G. Jeon, and W. Wu. Feedback network for image super-resolution. In *Proceedings of the IEEE Conference on Computer Vision and Pattern Recognition*, pages 3867–3876, 2019.
- [21] B. Lim, S. Son, H. Kim, S. Nah, and K. Mu Lee. Enhanced deep residual networks for single image super-resolution. In *Proceedings of the IEEE conference on computer vision and pattern recognition workshops*, pages 136–144, 2017.
- [22] J. Liu, W. Zhang, Y. Tang, J. Tang, and G. Wu. Residual feature aggregation network for image super-resolution. In *Proceedings of the IEEE/CVF Conference on Computer Vision and Pattern Recognition*, pages 2359–2368, 2020.
- [23] X. Luo, Y. Xie, Y. Zhang, Y. Qu, C. Li, and Y. Fu. Latticenet: Towards lightweight image super-resolution with lattice block.
- [24] A. Mehri, P. B. Ardakani, and A. D. Sappa. Mprnet: Multi-path residual network for lightweight image super resolution. *arXiv preprint arXiv:2011.04566*, 2020.
- [25] A. Muqet, J. Hwang, S. Yang, J. Kang, Y. Kim, and S.-H. Bae. Multi-attention based ultra lightweight image super-resolution. *arXiv preprint arXiv:2008.12912*, 2020.
- [26] B. Niu, W. Wen, W. Ren, X. Zhang, L. Yang, S. Wang, K. Zhang, X. Cao, and H. Shen. Single image super-resolution via a holistic attention network. In *European Conference on Computer Vision*, pages 191–207. Springer, 2020.

- [27] A. Paszke, S. Gross, S. Chintala, G. Chanan, E. Yang, Z. DeVito, Z. Lin, A. Desmaison, L. Antiga, and A. Lerer. Automatic differentiation in pytorch. 2017.
- [28] T. Peleg and M. Elad. A statistical prediction model based on sparse representations for single image super-resolution. *IEEE transactions on image processing*, 23(6):2569–2582, 2014.
- [29] P. Rodríguez, J. M. Gonfaus, G. Cucurull, F. XavierRoca, and J. Gonzalez. Attend and rectify: a gated attention mechanism for fine-grained recovery. In *Proceedings of the European Conference on Computer Vision (ECCV)*, pages 349–364, 2018.
- [30] W. Shi, J. Caballero, F. Huszár, J. Totz, A. P. Aitken, R. Bishop, D. Rueckert, and Z. Wang. Real-time single image and video super-resolution using an efficient sub-pixel convolutional neural network. In *Proceedings of the IEEE conference on computer vision and pattern recognition*, pages 1874–1883, 2016.
- [31] Y. Tai, J. Yang, and X. Liu. Image super-resolution via deep recursive residual network. In *Proceedings of the IEEE conference on computer vision and pattern recognition*, pages 3147–3155, 2017.
- [32] Y. Tai, J. Yang, X. Liu, and C. Xu. Memnet: A persistent memory network for image restoration. In *Proceedings of the IEEE international conference on computer vision*, pages 4539–4547, 2017.
- [33] T. Tong, G. Li, X. Liu, and Q. Gao. Image super-resolution using dense skip connections. In *Proceedings of the IEEE International Conference on Computer Vision*, pages 4799–4807, 2017.
- [34] G. Urban, K. J. Geras, S. E. Kahou, O. Aslan, S. Wang, R. Caruana, A. Mohamed, M. Philipose, and M. Richardson. Do deep convolutional nets really need to be deep and convolutional? *arXiv preprint arXiv:1603.05691*, 2016.
- [35] Q. Wang, B. Wu, P. Zhu, P. Li, W. Zuo, and Q. Hu. Ecanet: Efficient channel attention for deep convolutional neural networks. In *Proceedings of the IEEE/CVF Conference on Computer Vision and Pattern Recognition*, pages 11534–11542, 2020.
- [36] Y. Wang, F. Perazzi, B. McWilliams, A. Sorkine-Hornung, O. Sorkine-Hornung, and C. Schroers. A fully progressive approach to single-image super-resolution. In *Proceedings of the IEEE Conference on Computer Vision and Pattern Recognition Workshops*, pages 864–873, 2018.
- [37] S. Woo, J. Park, J.-Y. Lee, and I. So Kweon. Cbam: Convolutional block attention module. In *Proceedings of the European conference on computer vision (ECCV)*, pages 3–19, 2018.
- [38] R. Zeyde, M. Elad, and M. Protter. On single image scale-up using sparse-representations. In *International conference on curves and surfaces*, pages 711–730. Springer, 2010.
- [39] K. Zhang, X. Gao, D. Tao, and X. Li. Single image super-resolution with non-local means and steering kernel regression. *IEEE Transactions on Image Processing*, 21(11):4544–4556, 2012.
- [40] K. Zhang, W. Zuo, S. Gu, and L. Zhang. Learning deep cnn denoiser prior for image restoration. In *Proceedings of the IEEE conference on computer vision and pattern recognition*, pages 3929–3938, 2017.
- [41] L. Zhang and X. Wu. An edge-guided image interpolation algorithm via directional filtering and data fusion. *IEEE transactions on Image Processing*, 15(8):2226–2238, 2006.
- [42] Y. Zhang, K. Li, K. Li, L. Wang, B. Zhong, and Y. Fu. Image super-resolution using very deep residual channel attention networks. In *Proceedings of the European Conference on Computer Vision (ECCV)*, pages 286–301, 2018.
- [43] Y. Zhang, Y. Tian, Y. Kong, B. Zhong, and Y. Fu. Residual dense network for image super-resolution. In *Proceedings of the IEEE conference on computer vision and pattern recognition*, pages 2472–2481, 2018.
- [44] H. Zhao, X. Kong, J. He, Y. Qiao, and C. Dong. Efficient image super-resolution using pixel attention. *arXiv preprint arXiv:2010.01073*, 2020.
- [45] F. Zhu and Q. Zhao. Efficient single image super-resolution via hybrid residual feature learning with compact back-projection network. In *Proceedings of the IEEE International Conference on Computer Vision Workshops*, pages 0–0, 2019.